Commun. Comput. Phys.
doi: 10.4208/cicp.220513.151113a

Vol. **16**, No. 1, pp. 56-74
July 2014

Shape Recovery of Elastic Capsules from Shear Flow Induced Deformation

John Gounley and Yan Peng*

Department of Mathematics and Statistics, Old Dominion University, Norfolk, VA 23529, USA.

Received 22 May 2013; Accepted (in revised version) 15 November 2013

Available online 28 March 2014

Abstract. Red blood cells undergo substantial shape changes in vivo. Modeled as a viscoelastic capsule, their deformation and equilibrium behavior has been extensively studied. We consider how 2D capsules recover their shape, after having been deformed to 'equilibrium' behavior by shear flow. The fluid-structure interaction is modeled using the multiple-relaxation time lattice Boltzmann (LBM) and immersed boundary (IBM) methods. Characterizing the capsule's shape recovery with the Taylor deformation parameter, we find that a single exponential decay model suffices to describe the recovery of a circular capsule. However, for biconcave capsules whose equilibrium behaviors are tank-treading and tumbling, we posit a two-part recovery, modeled with a pair of exponential decay functions. We consider how these two recovery modes depend on the capsule's shear elasticity, membrane viscosity, and bending stiffness, along with the ratio of the viscosity of the fluid inside the capsule to the ambient fluid viscosity. We find that the initial recovery mode for a tank-treading biconcave capsule is dominated by shear elasticity and membrane viscosity. On the other hand, the latter recovery mode for both tumbling and tank-treading capsules, depends clearly on shear elasticity, bending stiffness, and the viscosity ratio.

AMS subject classifications: 74F10

Key words: Fluid-structure interaction, shape recovery, lattice Boltzmann method, immersed boundary method.

1 Introduction

The shape change of viscoelastic, fluid-filled capsules has received considerable attention by researchers in recent years. This attention has particularly centered on its application to red blood cells, which may be modeled in such a way. The passage of blood through

*Corresponding author. *Email addresses:* jgounley@odu.edu (J. Gounley), ypeng@odu.edu (Y. Peng)

small capillaries requires significant deformation by red blood cells, from the normal biconcave discoid to a bullet-like shape [30]. Upon reaching larger blood vessels, the red blood cells recover their normal shape. In blood diseases, such as sickle-cell anemia, the ability of red blood cells to deform and subsequently recover their shape is reduced. As a result, they may block capillaries and oxygen delivery may be adversely impacted [28]. To aid the development of treatments for such blood diseases, and to better understand the mechanical structure of red blood cells, it is important to study the manner in which their shape is deformed and recovered.

Extensive study has been made of the deformation of viscoelastic, fluid-filled capsules under shear flow. Blood flow *in vivo* is not archetypal shear flow, but this has become a standard venue for considering the shape change of red blood cells. Experimental and theoretical work [8, 21, 22] has been recently complemented by significant computational simulations [5, 30, 31]. Among studies focusing on a single capsule, the constitutive law governing the elastic character of the membrane has been investigated [2]. The role of the membrane's bending stiffness has been studied by boundary integral [18] and lattice Boltzmann methods [25]. The effect of different capsule and ambient viscosities on deformation has been discussed [20, 26], and considered in concert with membrane viscosity [29]. Recently, a strikingly novel volume-of-fluid method was introduced which has the advantage of doing without a separate structural grid [11].

Conversely, investigations into the shape recovery of capsules from deformation have been largely limited to experimental and theoretical avenues. These studies primarily aimed at measuring the time course of shape recovery and determining the dominant mechanisms by which it occurred. Micropipette aspiration has been used to induce a large deformation in part of the red blood cell membrane and allow that deformation to relax [7]. Complementing their experimental work with a theoretical analysis of micropipette aspiration, Evans and Hochmuth characterized the time course of this recovery with the exponential decay function $e^{-t/tc}$. Their work concluded that the time constant is given as $tc = \frac{2\eta_e}{E_s}$, where η_e is the capsule's membrane viscosity constant and E_s is the capsule shear elasticity modulus [7]. More recently, optical tweezing has been applied to study the relaxation of red blood cell membranes and showed behavior consistent with the exponential decay function characterization [4]. In their associated theoretical model of optical tweezing, similar to that for micropipette aspiration, Dao *et al.* also characterized tc as a ratio of η_e to E_s. Lastly, red blood cells have been placed in shear flow and deformed until reaching an equilibrium state. After abruptly stopping the shear flow, the time course of the shape recovery has been measured by the same exponential decay function [3]. Among other shear flow studies, Fischer showed that red blood cells possess a shape memory [8] and Sutera *et al.* suggested that the time constant tc may also depend on the ambient viscosity [27].

While relaxation from micropipette aspiration or optical tweezing may be a primarily solid mechanical process, as modeled in [4] and [7], the shape recovery from cell deformation in shear flow suggests that a similar characterization may be used to describe a more complex case of shape recovery [3]. Red blood cell deformation in shear flow having been

modeled as a fluid-structure interaction, as discussed above, implies that a comparable model and methodology would be appropriate to study the shape recovery from such a deformation. While the equations describing the fluid-structure interaction in shape recovery are not amenable to analytic solutions, a computational approach may be used to confirm the experimental behavior observed and better understand the parameters – potentially both structural and fluidic – on which tc depends.

In this work, we introduce a 2D model of capsule deformation in, and shape recovery from, shear flow. Our fluid-structure interaction model belongs to what Hou *et al.* denote the "partitioned" paradigm, with separate fluid and capsule meshes and algorithms [10]. A lattice Boltzmann method (LBM) is used to solve the fluid flow, while the immersed boundary method (IBM) is chosen to simulate the fluid-structure interaction. Validation of the model for the shear flow induced deformation of a circular capsule is given by comparison to previous models of capsule deformation. Subsequently, the model is used to simulate shape recovery after the abrupt stop of shear flow for various fluid and capsule parameters, for both circular and biconcave capsules. We find that while a exponential decay function $e^{-t/tc}$ fits the data very well for circular capsules, the recovery of biconcave capsules is best described by a pair of exponential decay functions, with different tc values.

2 Modeling and methodology

2.1 Model

We consider initially circular and biconcave fluid-filled 2D capsules in shear flow. A red blood cell has shear and isotropic elasticity, bending stiffness, and membrane viscosity [6, 7, 22]. The isotropic elasticity is not explicitly modeled here; the area increase in our simulations does not exceed 0.2% for circular capsules and falls in the range of $6-8\%$ for biconcave capsules. We model the shear elasticity of the capsule with Hooke's law. Expressed as

$$\tau_e = E_s(\lambda - 1), \tag{2.1}$$

τ_e is given in terms of shear elasticity modulus E_s and non-dimensional membrane stretch ratio $\lambda(t) = \frac{\ell(t)}{\ell_0}$, for arc length ℓ at time t and initial arc length ℓ_0 [25]. For the sake of comparison, we also considered neo-Hookean elasticity [2], as

$$\tau_e = \frac{2}{3}E_s(\lambda^{3/2} - \lambda^{-3/2}). \tag{2.2}$$

Additionally, the membrane viscosity is accounted for by the tension τ_v with a Kelvin-Voigt model, as

$$\tau_v = \eta_e \frac{1}{\lambda}\frac{\partial \lambda}{\partial t}, \tag{2.3}$$

for membrane viscosity constant η_e [29]. The time derivative of λ is calculated using an explicit one-sided second order finite difference method. Consequently, the total in-plane tension is

$$\tau = \tau_e + \tau_v. \tag{2.4}$$

Further, the bending stiffness creates transverse shear tension,

$$q = \frac{\partial m}{\partial \ell} = E_B \frac{\partial}{\partial \ell}(\kappa - \kappa_0), \tag{2.5}$$

in which we have bending modulus E_B, bending moment m, initial curvature κ_0, curvature $\kappa(t)$ at time t, and differentiation with respect to the arc length ℓ [18]. We calculate κ with periodic cubic spline interpolation. Consequently, the membrane stress at the interface is $\mathbf{T} = \tau\mathbf{t} + q\mathbf{n}$ and the corresponding tension jump is

$$\Delta F = -\frac{\partial \mathbf{T}}{\partial \ell} = -\frac{\partial}{\partial \ell}\left(\tau\mathbf{t} + q\mathbf{n}\right), \tag{2.6}$$

for unit vectors $\mathbf{t}$ and $\mathbf{n}$ which are tangent and normal to the interface, respectively. The necessary first and second derivatives with respect to arc length ℓ are calculated using five point centered finite difference methods for arbitrarily spaced grid points.

We focus our attention on four dimensionless parameters which affect deformation in and shape recovery from shear flow. First, the dimensionless shear rate G is the ratio of the fluid's shearing force to the capsule's elastic force and is calculated as

$$G = \frac{\mu_a u_0 a}{E_s}, \tag{2.7}$$

in which μ_a is the viscosity of the ambient fluid, u_0 is the characteristic velocity, and a is the equivalent capsule radius.

Second, we define the ratio of the membrane viscosity constant η_e to the viscosity of the fluid inside the capsule μ_c as

$$M = \frac{\eta_e}{a\mu_c}. \tag{2.8}$$

Third, the reduced ratio of bending to elasticity represents the relative impact of these two factors, as

$$E_b = \frac{E_B}{a^2 E_s}. \tag{2.9}$$

Additionally, the fluid inside the capsule may have different properties than the ambient fluid. For the case of red blood cells, the densities of the two fluids are nearly the same. However, the viscosity of the fluid inside the capsule is approximately five times the ambient viscosity. Consequently, the fourth dimensionless parameter investigated is the ratio of the viscosity of the fluid inside the capsule μ_c, to the ambient fluid viscosity μ_a, as the viscosity jump V, where

$$V = \frac{\mu_c}{\mu_a}. \tag{2.10}$$

2.2 Numerical methods

Our numerical methodology combines the lattice Boltzmann and immersed boundary methods. Derived from the Boltzmann equation of statistical mechanics, the lattice Boltzmann method considers the fluid to be sets of particles that move between lattice nodes in discrete timesteps. The expression $f_i(\mathbf{x}_j,t_n)$ represents the distribution of particles at $\mathbf{x}_j$ with velocity $\mathbf{c}_i$ at time t_n. The discrete velocities $\mathbf{c}$ are from the D2Q9 lattice model and we set $\delta x=\delta t$. Using the multiple relaxation time (MRT) approximation of the collision integral, we have the lattice Boltzmann equation

$$\mathbf{f}(\mathbf{x}_j+\mathbf{c}\delta_t,t_n+\delta_t)-\mathbf{f}(\mathbf{x}_j,t_n)=-M^{-1}\hat{S}[\mathbf{m}(\mathbf{x}_j,t_n)-\mathbf{m}^{(eq)}(\mathbf{x}_j,t_n)], \tag{2.11}$$

in which $\mathbf{f}$, $\mathbf{m}$, and $\mathbf{m}^{(eq)}$ represent the vectors whose components are the distribution functions with each particle velocity $\mathbf{c}$, the velocity moments, and the equilibrium moments, respectively [16]. Additionally, the matrix M maps from probability distribution space into moment space, and $\hat{S}$ is the diagonal matrix of relaxation rates $[s_1,s_2,\cdots,s_9]$ [13]. The relaxation rates s_1,s_4 and s_6 for the conserved moments have no effect for the model. For D2Q9 model, the shear viscosity ν is $\nu=\frac{1}{3}(\frac{1}{s_8}-\frac{1}{2})c\delta x$. It is required that $s_8=s_9$ and $s_5=s_7$. The relaxation rates $s_5=s_7$ can affect the accuracy of the boundary conditions and are determined by $s_5=s_7=8\frac{2-s_8}{8-s_8}$ [9]. The other relaxation rates s_2 and s_3 do not affect the hydrodynamics in the lowest order approximation and only affect the small scale behaviour of the model. Usually they are determined by the linear stability analysis. We use $s_2=s_3=1.64$ [12].

The immersed boundary method was developed by Peskin [17] and integrated into the MRT lattice Boltzmann method by Peng and Luo [16]. Keeping the Eulerian fluid domain constant, a Lagrangian mesh is used to describe the motion of the capsule. The interaction of the fluid and structure is performed by using the local fluid velocity to update the location of the capsule boundary, while forces created by capsule deformation are distributed to the nearby fluid nodes. We employ a 2D version of the discrete delta function, which is defined as

$$\delta_h(\mathbf{x})=\delta_h(x_1)\delta_h(x_2)\cdots\delta_h(x_d),\quad \mathbf{x}\in R^d, \tag{2.12}$$

$$\delta_h(x)=\begin{cases}\frac{1}{4h}\left[1+\cos(\frac{\pi x}{2h})\right], & |x|\le 2h,\\ 0, & |x|>2h\end{cases} \tag{2.13}$$

to transfer data between the two grids. Denoting a Lagrangian capsule node position as $\mathbf{X}_c$, Eulerian grid points by $\mathbf{x}_j$, and the Eulerian fluid velocities as $\mathbf{u}_j$, then we determine the capsule velocity $\mathbf{U}$ at $\mathbf{X}_c$ by

$$\mathbf{U}(\mathbf{X}_c)=\sum_j\delta(\mathbf{X_c}-\mathbf{x}_j)\mathbf{u}_j, \tag{2.14}$$

and update its location using the forward Euler method,

$$\mathbf{X_c}(t+\Delta t)=\mathbf{X_c}(t)+\mathbf{U}(\mathbf{X_c}(t))\Delta t. \tag{2.15}$$

Conversely, the capsule forces $\mathbf{F}(\mathbf{X_c})$ are distributed so that the fluid forces $\mathbf{f}(\mathbf{x_j})$ are

$$\mathbf{f}(\mathbf{x_j}) = \sum_c \delta(\mathbf{X_c} - \mathbf{x}_j)(\mathbf{F}(\mathbf{X_c})). \tag{2.16}$$

For dealing with the fluid viscosity jump across the capsule interface, we adopt the strategy of [30]. To determine the viscosity of a fluid node at a given timestep, we select the Lagrangian node nearest to the fluid node. The dot product of the vector between these two points and the unit outward normal from the Lagrangian node is calculated and the sign of this dot product produces a reliable indication of whether the fluid node is inside or outside of the capsule. Next, we approximate the shortest (normal) distance d from the fluid node to the capsule boundary. The sign of d is set to be positive if located outside of the capsule, or negative if inside of the capsule. Subsequently, we introduce a Heaviside function of d from [30],

$$H(d) = \begin{cases} 0, & d < -2h, \\ \frac{1}{2}\left(1 + \frac{d}{2h} + \frac{1}{\pi}\sin\frac{\pi d}{2h}\right), & -2h \le d \le 2h, \\ 1, & d > 2h. \end{cases} \tag{2.17}$$

Finally, the viscosity μ at the node is given in terms of $H(d)$ by the equation

$$\mu(x) = \mu_c + (\mu_a - \mu_c)H[d(\mathbf{x})]. \tag{2.18}$$

2.3 Validation

To validate the model and methods used, we compared our results with an existing 2D model for deformation of circular capsules. The comparison was made with respect to the Taylor deformation parameter

$$D_{xy} = \frac{L - W}{L + W}, \tag{2.19}$$

for capsule length L and width W. In our work, L and W were measured as the longest and shortest axes of the capsule at the given timestep. We also compared the capsule's angle of inclination θ, measured with respect to the horizontal direction of flow.

The comparison was made with Sui and coworkers [24, 25], who used a multiblock BGK-LBM model in concert with the immersed boundary method. These works used Hookean elasticity and included membrane stiffness, but did not address membrane viscosity or the viscosity jump. In Figs. 1(a) and 1(b), we consider different shear rates in the absence of bending resistance. Although our simulations somewhat overshot the equilibrium D_{xy} values for higher shear rates, there was consistent agreement between the two methods. Additionally, we considered the shear rate $G = 0.04$ with various bending to elasticity ratios in Figs. 2(a) and 2(b). Our results for the impact of bending stiffness matched quite well, excepting a slight wobble in the angle of inclination for $E_b = 0.2$.

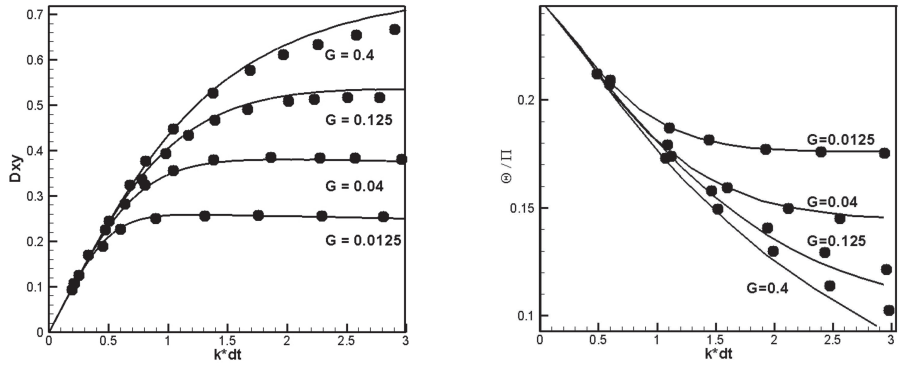

(a) D_{xy} for various G (b) $\frac{\theta}{\pi}$ for various G

Figure 1: The Taylor deformation parameter and inclination angle are graphed against time, where circles represent data points from [24] and the solid lines are the results of our simulations. Figs. 1(a) and 1(b) show $G=0.0125$, 0.04, 0.125, and 0.4, where $E_b=0$, $V=1$, and $M=0$.

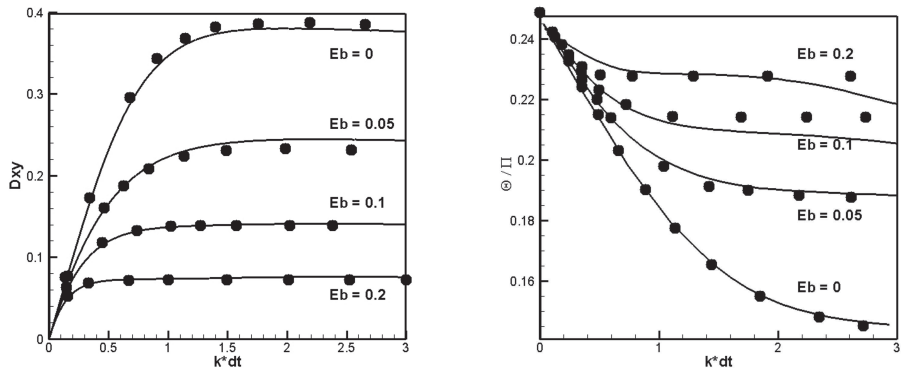

(a) D_{xy} for various E_b (b) $\frac{\theta}{\pi}$ for various E_b

Figure 2: The Taylor deformation parameter and inclination angle are graphed against time, where circles represent data points from [25] and the solid lines are the results of our simulations. Figs. 2(a) and 2(b) show $E_b=0$, 0.05, 0.1, and 0.2, where $G=0.04$, $V=1$, and $M=0$.

2.4 Setup

We considered a rectangular domain, with 321 nodes in the dimension of the shear flow and 241 nodes in the transverse direction. The uniform lattice size was $h=0.25\mu m$ and the timestep $\Delta t=0.25\mu s$, and a Reynolds number of 0.05 was used. The capsule boundary is discretized into 140 Lagrangian nodes, such that each segment is initially of equal length. The initial shear flow, continuously enforced on the domain boundaries, is $\vec{u}=(ky,0)$, for shear rate $k=10s^{-1}$ and $y\in[-H,H]$ where H is half of the transverse length. Capsule deformation and shape recovery are studied in terms of the Taylor deformation param-

eter. Our choice of the Taylor deformation parameter was guided by two factors: (1) its widespread use in computational studies of capsule deformation and (2) that it characterizes (however imperfectly) the entire capsule shape.

3 Circular capsules

An initially unstressed circular capsule was placed in the center of the shear flow domain. The capsule was deformed by the flow until the system reached a clear equilibrium. Initially zero, the Taylor deformation parameter D_{xy} increases during this process to a constant equilibrium value, as shown in Figs. 1(a) and 2(a), which we denote D_0. At this point, the boundary conditions driving the shear flow were stopped and the capsule gradually relaxed toward its initial shape, corresponding to $D_\infty = 0$. This simulation was performed for a variety of four dimensionless parameters: G, M, E_b, and V.

We found that, as suggested by [3], the decay in the Taylor deformation parameter was approximately exponential. For each set of simulation parameters, the exponential curve $e^{-\frac{t}{tc}}$ which best fit the decay in D_{xy} from D_0 was calculated using a least squares method. Fig. 3 shows examples of simulation data points plotted against $e^{-\frac{t}{tc}}$ for their respective values of tc and suggests that the exponential decay function is suffices to describe the recovery.

Analysis of our results showed that the time constant tc clearly depended not only on the shear rate G and membrane to fluid viscosity ratio M, but also on the reduced bending modulus E_b and viscosity jump V. We found that G, M, and V had linear relationships

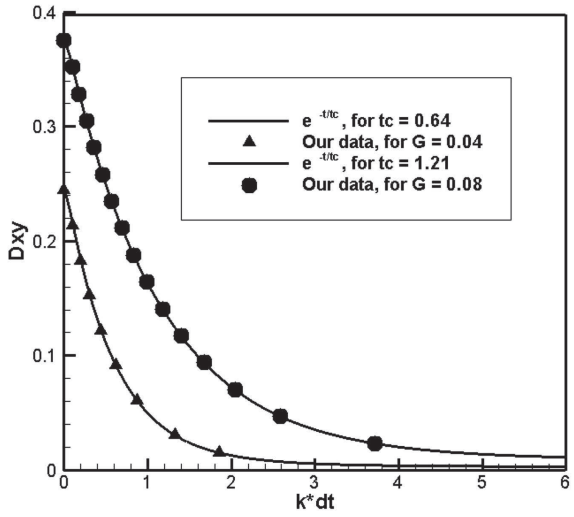

Figure 3: Simulation data points plotted against exponential decay curves for calculated values of tc. Other parameters were $E_b = 0.05$, $V = 1$, and $M = 0$.

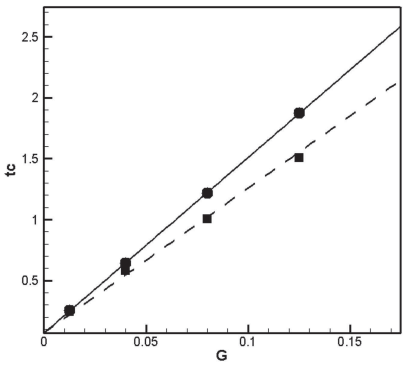

(a) Other parameters are $E_b = 0.05$, $V = 1$, and $M = 0$

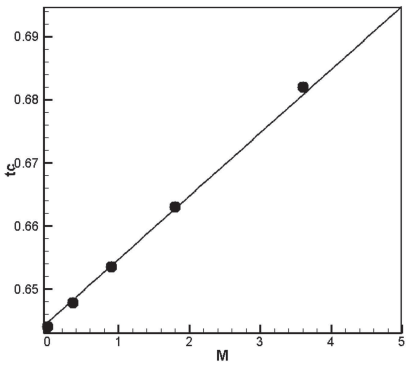

(b) Other parameters are $G = 0.04$, $E_b = 0.05$, and $V = 1$

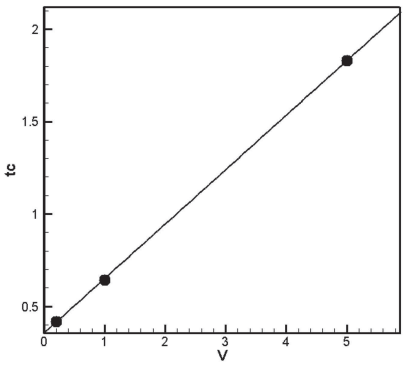

(c) Other parameters are $G = 0.04$, $E_b = 0.05$, and $M = 0$

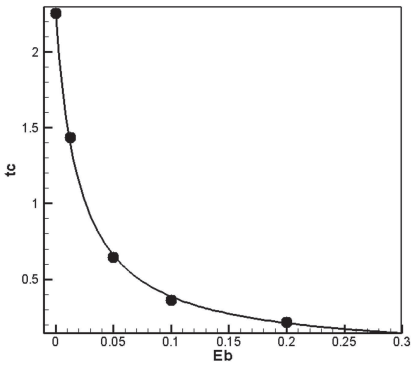

(d) Other parameters are $G = 0.04$, $V = 1$, and $M = 0$

Figure 4: Circles represent tc values from simulations varying (a) shear rate G, (b) membrane to fluid viscosity ratio M, (c) viscosity jump V, and (d) bending stiffness E_b. Squares in (a) represent tc values for neo-Hookean elasticity.

with tc, while E_b was inversely proportional with it, as illustrated in Fig. 4. Despite this common linearity, the relative importance of the three linear parameters differed widely: tc varies directly with G, while increases in M have minimal impact on tc and the role of V is somewhere between these two. Bending stiffness also has a large role for small values of E_b.

One might write an approximate function for the time constant as $tc = \rho \frac{G(V+\phi)}{E_b}$, for constants ρ and ϕ. Yet the simplifications due to the capsule's circularity are clear, in the near-irrelevance of membrane viscosity and the shape recovery of a capsule which lacked bending stiffness and, therefore, a preferred curvature. The largely linear course of shape recovery of a circular capsule seems the mirror image of its deformation.

4 Biconcave capsules

We contrast our results for a simple circular capsule with a biconcave capsule, described by the equation

$$x = a\alpha \sin\chi, \tag{4.1}$$

$$y = a\frac{\alpha}{2}(0.207 + 2.003\sin^2\chi - 1.123\sin^4\chi)\cos\chi, \tag{4.2}$$

for cell radius ratio $\alpha = 1.29$, characteristic length $1.48a$, and χ ranging from -0.5π to 1.5π.

When deformed in shear flow, a biconcave capsule has been shown in computational and experimental studies to have (at least) two distinct 'equilibrium' behaviors: tumbling and tank-treading [1, 8, 23]. In tumbling, the capsule continuously tumbles forward, with its shape undergoing periodic changes but retaining its biconcavity. Conversely, tank-treading involves deformation of the capsule to a near constant shape and angle of inclination, with a near-periodic rotation of the membrane around the internal fluid. Simulations have shown that the shear rate, bending stiffness, membrane viscosity, and the viscosity jump all play some role in determining the capsule's equilibrium behavior [15, 23, 25]. Given the very different deformations involved, we consider the recoveries of tank-treading and tumbling capsules separately.

After deformation to equilibrium behavior, we found that both tank-treading and tumbling capsules returned to their initial shapes, presuming $E_b > 0$. The only mechanism by which a 2D capsule may express a shape preference is bending stiffness, as opposed to a 3D capsule in which shear elasticity is an additional mechanism. For $E_b = 0$, we found that after stopping the shear flow, capsules briefly changed to a slightly more circular shape, but underwent no further shape change, as illustrated in Fig. 5.

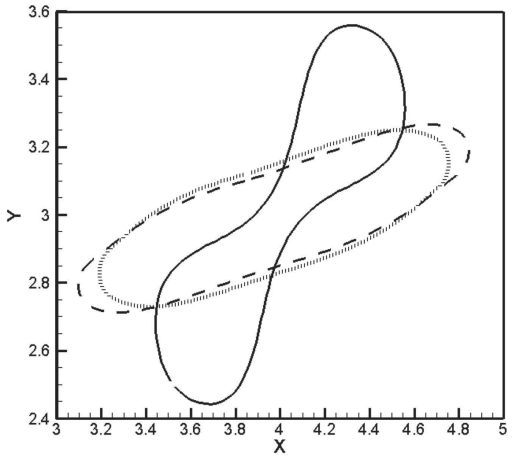

Figure 5: For capsule with no bending stiffness, we compare shapes when undeformed (solid line), when flow stops (dashed line), and after recovery (dotted line).

4.1 Tank-treading

Our results suggest that there are two separate modes in the shape recovery process of a tank-treading capsule. First, there is a brief period of relaxation, in which energy is quickly dissipated and the Taylor deformation parameter sharply decreases from D_0 to $D_{\min}$. Second, there follows a much slower period of relaxation, in which the Taylor deformation parameter increases from $D_{\min}$ to its initial value D_∞. We illustrate the complete recovery process in Fig. 6(a), in which A, B, and C denote the positions of D_0, $D_{\min}$, and D_∞, respectively. The corresponding capsule shapes are shown in Fig. 6(b), with the solid curve representing D_0 (the initial shape), the dashed curve for $D_{\min}$ (the shape with the minimum D_{xy}), and the dotted curve denoting D_∞ (the final, recovered shape). We see that the initial recovery from the oblong tank-treading shape shortens the capsule, though it is only starting to exhibit biconcavity. Conversely, the latter part of the recovery process involves major changes in curvature and a large decrease in the capsule's width, to return to its biconcave shape.

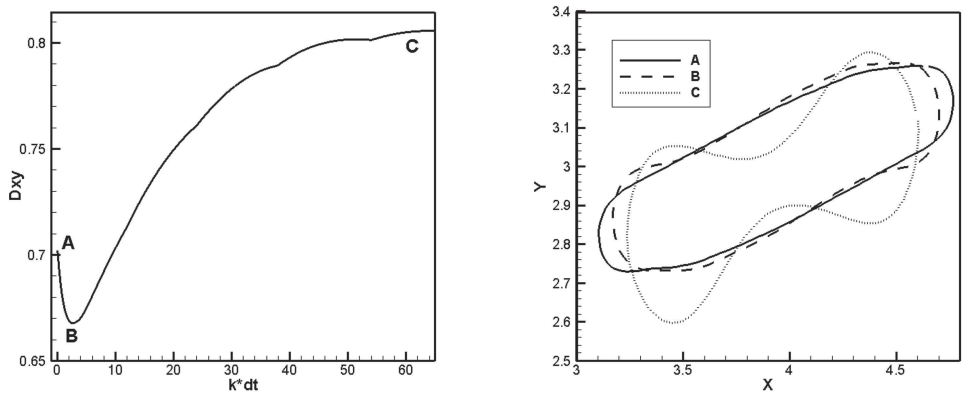

(a) (b)

Figure 6: Recovery from tank-treading in terms of (a) D_{xy} and (b) capsule shape.

To consider the dominant mechanisms of these two modes, we fitted the curves from D_0 to $D_{\min}$, and from $D_{\min}$ to D_∞, with exponential decay functions $e^{-\frac{t}{tc}}$. Calculations for the initial and latter tc values were found to be $\mathcal{O}(10^{-1})$ and $\mathcal{O}(10)$, respectively. Subsequently, the dependence of the resulting tc values on G, M, V, and E_b was studied.

We found that, for both the initial and latter recovery modes, tc was again directly proportional with G. A similar direct proportionality prevailed for the dependence of the latter tc on V, while increasing V produced only modest linear increases in the initial tc. Alternately, the initial tc has a strong dependence on M, while the latter tc was nearly independent of the M value. Finally, E_b has no clear relationship with the initial tc, but the latter tc has a clear inverse dependence on E_b. Data illustrating these results is found in Fig. 7.

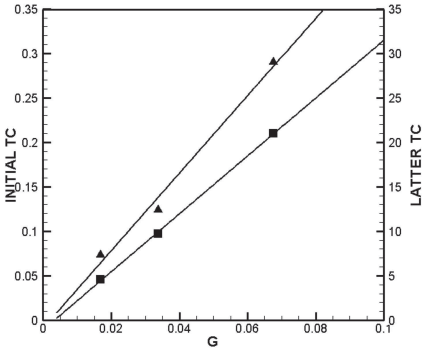

(a) Other parameters are $E_b = 0.0014$, $V = 1$, $M = 0$

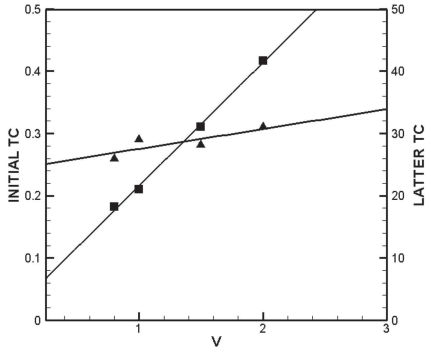

(b) Other parameters are $G = 0.067$, $E_b = 0.0014$, and $M = 0$

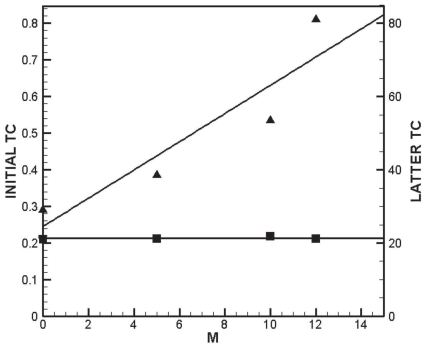

(c) Other parameters are $G = 0.067$, $E_b = 0.0014$, and $V = 1$

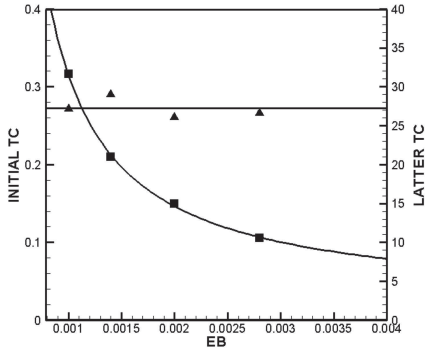

(d) Other parameters are $G = 0.067$, $V = 1$, and $M = 0$

Figure 7: For a tank-treading capsule, initial tc values (triangles) and latter tc values (squares) are compared for different G, V, M, and E_b. Solid lines approximate the relationship between the parameter and tc.

In summary, we see that the first mode is dominated by the elasticity and viscosity of the membrane, which cause the relaxation of the principal stretch ratio λ toward its equilibrium value of unity. Conversely, the elasticity and bending stiffness of the membrane, along with dissipation in the fluid, drive the second relaxation mode, which is dominated by the tank-treading and curvature changes necessary to regain the biconcave shape.

This initial recovery mode is consistent with theoretical and experimental results for recovery from micropipette aspiration and other deformations. We found that the initial $tc \approx \rho GM$, for constant ρ, as the roles of E_b and (to a lesser extent) V are small enough to be ignored, as argued in [7]. When stated in terms of the membrane's elasticity modulus and viscosity coefficient, this equation takes the form of initial $tc \approx \rho \frac{\eta_e}{E_s}$, which is the relationship suggested by Evans and Hochmuth, among others [3, 4, 7]. On the other hand, an equation for the latter tc might be written as $tc \approx \rho \frac{GV}{E_b - \phi}$, with the constant $\phi \ll 1$

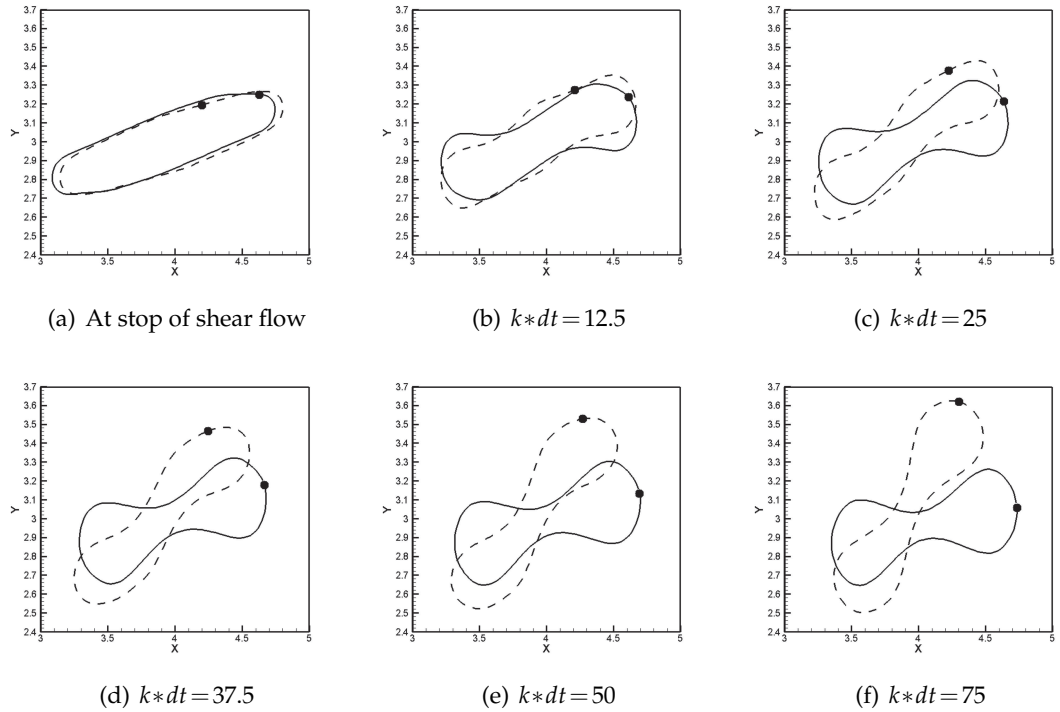

(a) At stop of shear flow (b) $k*dt=12.5$ (c) $k*dt=25$

(d) $k*dt=37.5$ (e) $k*dt=50$ (f) $k*dt=75$

Figure 8: We compare the shape recovery of capsules with phase differences of 0.11 (solid line) and 0.49 (dashed line) radians. Circles are the current location of an element initially at the end of each capsules.

representing the necessity that $E_b > 0$ for the capsule to recover its shape. In particular, the larger E_b is, the quicker the cell recovers its shape.

As the tank-treading capsule maintains an approximately constant angle of inclination, the course of shape recovery was also highly dependent on the position of the membrane at the time at which shearing was stopped. This was due to what Fischer denotes shape memory: a given element of the capsule returns to the same (or opposite, homologous) position it held prior to the deformation [8]. Adopting the definition by Le [14], we quantify the position of the membrane in terms of its phase angle $\beta(t) = \alpha(t) - \theta(t) - [\alpha_0 - \theta_0]$, in which $\alpha(t)$ and $\theta(t)$ are the current inclinations with respect to the flow field of the membrane element and capsule's major axis, respectively, and α_0 and θ_0 are the initial values of these angles. If phase angle β is small, then the capsule will recover its shape more quickly than for a larger phase angle. To control for this effect, the ensemble of above simulations were conducted with $\beta = 0.49$ radians.

Fig. 8 considers the recovery of tank-treading capsules with phase angles β of 0.11 and 0.49 radians, but identical parameters otherwise. Note in Fig. 8 that this phase angle determines the capsule's angle of inclination after shape recovery. In contrast, one might have envisioned a recovery process consisting largely of tank-treading, in which the capsule maintained a constant angle of inclination.

4.2 Tumbling

Unlike initially biconcave tank-treading capsules, the shape recovery process for tumbling capsules typically involves the Taylor deformation parameter decreasing or increasing monotonically to its initial value. Whether decreasing or increasing occurs is determined by the angle of inclination θ of the capsule's major axis when the shear flow is stopped. In Fig. 9(a), the solid and dashed lines depict the capsule's recovery for angles $-\frac{\pi}{3}$ and $\frac{\pi}{6}$, respectively. To facilitate comparisons, the following simulations were conducted with an angle of $-\frac{\pi}{3}$ when the shear flow is stopped.

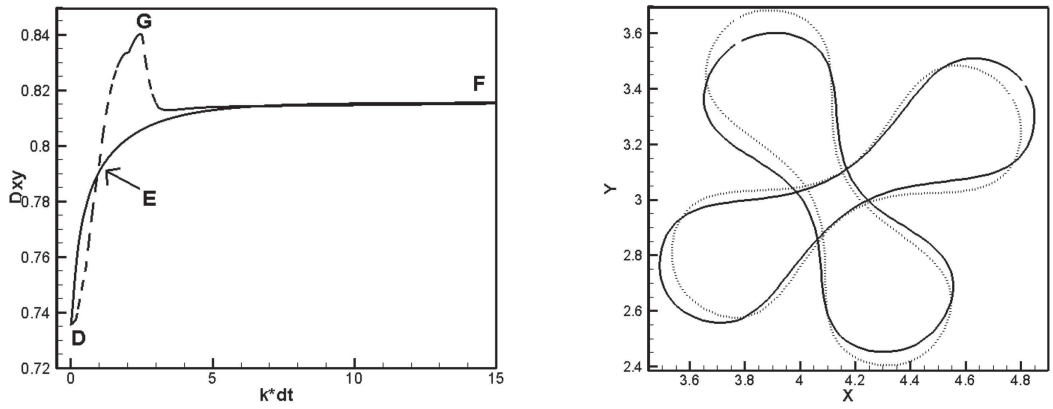

(a) (b)

Figure 9: In (a), we compare shape recovery in terms of D_{xy} for stopping flow at differing angles of inclination, $-\frac{\pi}{3}$ (time D) and $\frac{\pi}{6}$ (time G), with solid and dashed lines, respectively. Time E denotes the transition between initial and latter recovery modes for the capsule stopped at $-\frac{\pi}{3}$. In (b), we consider the capsule shapes when flow is stopped (solid lines, taken at times D and G) and upon recovery (dotted lines, at time F). Both capsules share $G=0.04$, $E_b=0.05$, $M=0$, and $V=2$.

Despite this monotonicity, a single exponential decay function $e^{-\frac{t}{tc}}$ failed to model D_{xy}'s recovery as completely as for circular capsules. Rather, as with tank-treading capsules, there seemed be a brief, initial mode of rapid recovery, followed by a more gradual relaxation of the Taylor deformation parameter to its initial value. Consequently, we modeled the recovery with a pair of exponential decay functions, estimating when the change in recovery modes occurred. The difference in the order of magnitude for the calculated tc values was smaller than for tank-treading capsules, with the initial tc being $\mathcal{O}(10^{-1}-10^{0})$ and the latter tc being $\mathcal{O}(10^{0}-10^{1})$.

As Fig. 10 illustrates, both initial and latter tc values were directly proportional with G. The latter tc was also directly proportional with V, while the initial tc had a much less steep linear relationship with V. Increases in M also produced modest, somewhat linear increases in both tc values. Lastly, the latter tc was relatively inversely proportional to E_b, while only a very small E_b had a meaningful effect on the initial tc.

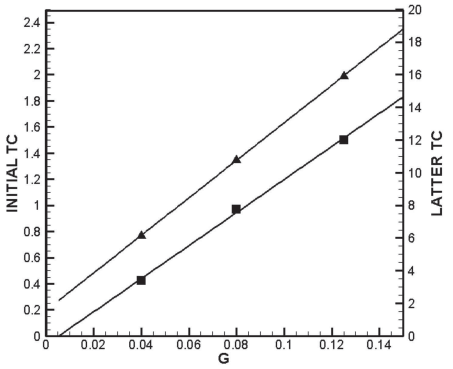

(a) Other parameters are $E_b=0.05$, $V=5$, $M=0$

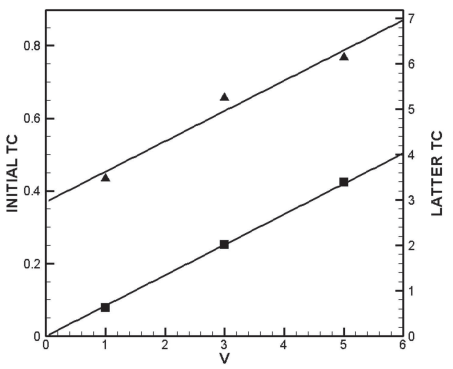

(b) Other parameters are $G=0.04$, $E_b=0.05$, and $M=0$

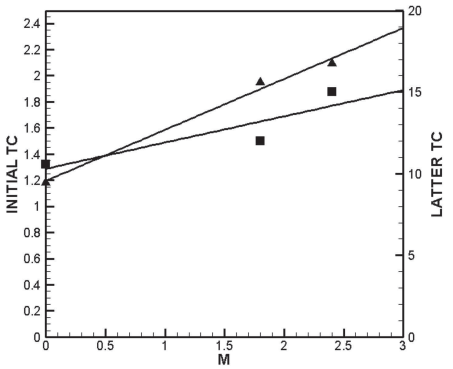

(c) Other parameters are $G=0.04$, $E_b=0.0125$, and $V=5$

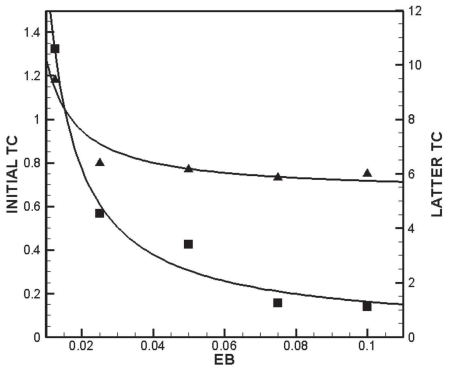

(d) Other parameters are $G=0.04$, $V=5$, and $M=0$

Figure 10: For a tumbling capsule, initial tc values (triangles) and latter tc values (squares) are compared for different G, V, M, and E_b. Solid lines approximate the relationship between the parameter and tc.

Suggesting an approximation of the initial tc for tumbling capsules is difficult, given its imprecise relationships with parameters other than G. Even bending stiffness impacts the initial tc, in sharp contrast to the tank-treading case. Conversely, the equation of the latter $tc \approx \rho \frac{GV}{E_b - \phi}$ given for a tank-treading capsule again provides a reasonable model for the data from tumbling capsules, though it fails to account for the modest role of M in this recovery mode.

4.3 Discussion

Our results differ from previous studies in their consideration of the entire shape recovery process. In the work of Evans and Hochmuth, Dao *et al.*, and others, they consider

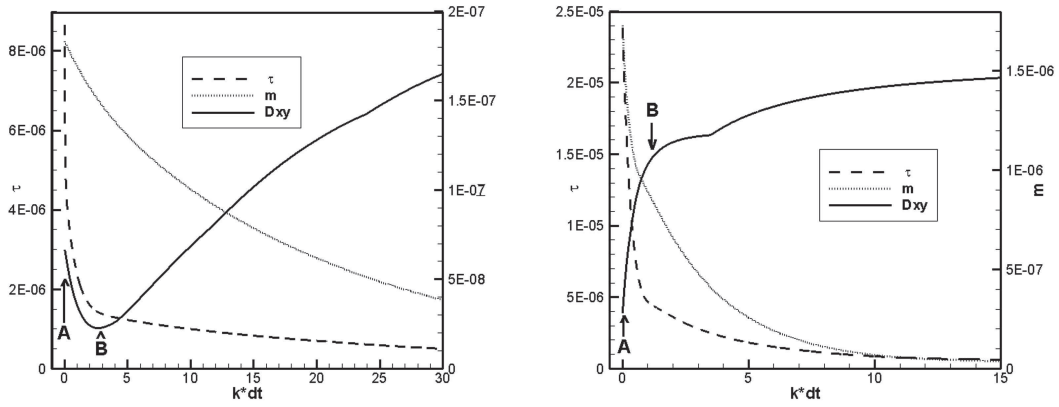

(a) (b)

Figure 11: Comparison of tension τ (left axis), bending moment m (right axis), and Taylor deformation parameter (axis not shown) during shape recovery. For the sake of clarity, only part of the recovery time is shown in (a).

recovery with respect to the principal stretch ratio λ and found $tc = \rho \frac{\eta_e}{E_s}$, for a constant ρ. This is consistent with our result for tc for the initial recovery from tank-treading, but fails to accommodate the major shape changes which a tank-treading capsule must undergo later in its shape recovery from shear flow. This may be seen by comparing the changes in membrane tension τ and bending moments m after the stop of shear flow to the Taylor deformation parameter. In Fig. 11, this comparison is made for (a) tank-treading and (b) tumbling capsules, with shear flow stopped at time A. We see that, for the tank-treading capsule, membrane tension is very quickly dissipated, and that this occurs while the Taylor deformation parameter decreases to its minimum value at time B, which we characterized as the first recovery mode. Subsequently, with little change in tension, bending moments continue their slow decrease, the course of which we called the second recovery mode. This distinction between modes is less clear for a tumbling capsule: while tension is again quickly dissipated after shear flow stops at time A, the relatively larger bending stiffness of a tumbling capsule ensures that the decline of bending moments does not lag far behind. This pair of sharp declines conclude the first recovery mode at time B, after which both tension and bending moments gently decline to zero during the second recovery mode.

5 Summary

We have introduced a method for simulating the deformation and shape recovery of viscoelastic, fluid-filled capsules which uses the multiple relaxation time lattice Boltzmann and immersed boundary methods. We found that a single exponential decay function sufficed to describe the shape recovery of a circular capsule, in terms of the Taylor de-

formation parameter and in which the time constant was a clear function of the capsule's shear elasticity and bending stiffness, along with the viscosity jump. When this model was extended to biconcave capsules recovering from tank-treading or tumbling, we found that a more complicated recovery model was necessary.

Consequently, we have posited a two-part recovery for both tank-treading and tumbling biconcave capsules. The first mode, focused on dissipating large inter-membrane forces quickly, involves λ nearly returning to its initial value and is due to the membrane's elasticity and viscosity. The second mode, unnecessary for the smaller deformations which occur in micropipette aspiration, dissipates remaining forces while membrane elements return to their initial positions. For this latter mode, we found that shear elasticity, viscosity jump, and bending stiffness played significant – and almost identical – roles for both tank-treading and tumbling capsules.

These results are, inevitably, limited by the 2D model. The requirement that a non-circular capsule have a preference for its initial curvature in order to recover its shape may overstate the role of bending stiffness in shape recovery. Additionally, using a Skalak constitutive law, rather than a Hookean or neo-Hookean, would allow the role of the capsule's isotropic elasticity to be considered, which may also alter our findings. With respect to red blood cells in particular, 3D simulations are required to address the potential mechanisms of the cell shape memory. As it is not clear that red blood cells have a non-constant preferred curvature, computational studies with uniform curvature preferences have been conducted (e.g. [32]). A shape recovery study with a uniform curvature preference might help clarify the role of the red blood cell's elastic character in determining its biconcave discoidal shape, in line with recent studies [8, 19].

Acknowledgments

Y. Peng acknowledges support from Old Dominion University Research Foundation Grant #503921 and National Science Foundation Grant #1319078. J. Gounley acknowledges support from the Old Dominion University Modeling and Simulation Initiative.

References

[1] M. Abkarian, M. Faivre, and A. Viallat, Swinging of red blood cells under shear flow, Physical Review Letters, 98 (2007), pp. 188302-1–188302-4.

[2] D. Barthes-Biesel, A. Diaz, and E. Dhenin, Effect of constitutive laws for two-dimensional membranes on flow-induced capsule deformation, Journal of Fluid Mechanics, 460 (2002), pp. 211–222.

[3] O. Baskurt and H. Meiselman, Determination of red blood cell shape recovery time constant in a couette system by the analysis of light reflectance and ektacytometry, Biorheology, 33 (1996), pp. 487–501.

[4] M. Dao, C. Lim, and S. Suresh, Mechanics of the human red blood cell deformed by optical tweezers, Journal of the Mechanics and Physics of Solids, 51 (2003), pp. 2259–2280.

[5] M. Dupin, I. Halliday, C. Care, L. Alboul, and L. Munn, Modeling the flow of dense suspensions of deformable particles in three dimensions, Physical Review E, 75 (2007), pp. 066707-1–0667070-17.
[6] E. Evans, Bending elastic modulus of red blood cell membrane derived from buckling instability in micropipet aspiration tests, Biophysical Journal, 43 (1983), pp. 27–30.
[7] E. Evans and R. Hochmuth, Membrane viscoelasticity, Biophysical Journal, 16 (1976), pp. 1–11.
[8] T. Fischer, Shape memory of human red blood cells, Biophysical Journal, 86 (2004), pp. 3304–3313.
[9] I. Ginzbourg and P. Adler, Boundary flow condition analysis for the three-dimensional lattice Boltzmann method, J. Phys. II, 4 (1994), pp. 191–214.
[10] G. Hou, J. Wang, and A. Layton, Numerical methods for fluid-structure interaction – a review, Commun. Comput. Phys., 12 (2012), pp. 337–377.
[11] S. Ii, X. Gong, K. Sugiyama, J. Wu, H. Huang, and S. Takagi, A full Eulerian fluid-membrane coupling method with a smoothed volume-of-fluid approach, Commun. Comput. Phys., 12 (2012), p. 544.
[12] P. Lallemand and L.-S. Luo, Theory of the lattice Boltzmann method: Dispersion, dissipation, isotropy, galilean, invariance, and stability, Physical Review E, 61 (2000).
[13] P. Lallemand, L.-S. Luo, and Y. Peng, A lattice Boltzmann front-tracking method for interface dynamics with surface tension in two dimensions, Journal of Computational Physics, 226 (2007), pp. 1367–1384.
[14] D. V. Le, Effect of bending stiffness on the deformation of liquid capsules enclosed by thin shells in shear flow, Physical Review E, 82 (2010), p. 016318.
[15] H. Noguchi and G. Gompper, Dynamics of fluid vesicles in shear flow: Effect of membrane viscosity and thermal fluctuations, Physical Review E, 72 (2005), p. 011901.
[16] Y. Peng and L.-S. Luo, A comparative study of immersed-boundary and interpolated bounce-back methods in LBE, Progress in Computational Fluid Dynamics, 8 (2008), pp. 156–167.
[17] C. Peskin, The immersed boundary method, Acta Numerica, 11 (2002), pp. 479–517.
[18] C. Pozrikidis, Numerical simulation of the flow-induced deformation of red blood cells, Annals of Biomedical Engineering, 31 (2003), pp. 1194–1205.
[19] C. Pozrikidis, Resting shape and spontaneous membrane curvature of red blood cells, Mathematical Medicine and Biology, 22 (2003), pp. 34–52.
[20] S. Ramanujan and C. Pozrikidis, Deformation of liquid capsules enclosed by elastic membranes in simple shear flow: large deformations and the effect of fluid viscosities, Journal of Fluid Mechanics, 361 (1998), pp. 117–143.
[21] T. Secomb, T. Fischer, and R. Skalak, The motion of close-packed red blood cells in shear flow, Biorheology, 20 (1983), pp. 283–294.
[22] R. Skalak, A. Tozeren, R. Zarda, and S. Chien, Strain energy function of red blood cell membranes, Biophysical Journal, 13 (1973), pp. 245–264.
[23] J. Skotheim and T. Secomb, Red blood cells and other nonspherical capsules in shear flow: Oscillatory dynamics and the tank-treading-to-tumbling transition, Physical Review Letters, 98 (2007), pp. 078301-1–078301-4.
[24] Y. Sui, A numerical study on the deformation of liquid-filled capsules with elastic membranes in simple shear flow, Ph.D. thesis, National University of Singapore, 2008.
[25] Y. Sui, Y. Chew, P. Roy, X. Chen, and H. Low, Transient deformation of elastic capsules in shear flow: Effect of membrane bending stiffness, Physical Review E, 75 (2007), pp. 066301-

1–066310-10.
[26] Y. Sui, H. Low, Y. Chew, and P. Roy, A front-tracking lattice Boltzmann method to study flow-induced deformation of three-dimensional capsules, Computers and Fluids, 39 (2010), pp. 499–511.
[27] S. Sutera, E. Mueller, and G. Zahalak, Extensional recovery of an intact erythrocyte from tan-treading motion, Journal of Biomedical Engineering, 112 (1990), pp. 250–256.
[28] S. Usami, S. Chien, P. Scholtz, and J. Bertles, Effect of deoxygenation on blood rheology in sickle cell disease, Microvascular Research, 9 (1975), pp. 324–334.
[29] J. Zhang, Effect of suspending viscosity on red blood cell dynamics and blood flows in microvessels, Microcirculation, 18 (2011), pp. 562–573.
[30] J. Zhang, P. Johnson, and A. Popel, An immersed boundary lattice Boltzmann approach to simulate deformable liquid capsules and its application to microscopic blood flows, Physical Biology, 4 (2007), pp. 285–295.
[31] J. Zhang, P. Johnson, and A. Popel, Red blood cell aggregation and dissociation in shear flows simulated by lattice Boltzmann method, Journal of Biomechanics, 41 (2008), pp. 47–55.
[32] M. Zhao and P. Bagchi, Dynamics of microcapsules in oscillating shear flow, Physics of Fluids, 23 (2011), p. 111901.